



# Highly efficient plasmonic dye-sensitized solar cells with silver nanowires and TiO<sub>2</sub> nanofibres incorporated multi-layered photoanode

M.G.C.M. Kumari<sup>a</sup>, C.S. Perera<sup>a</sup>, B.S. Dassanayake<sup>a</sup>, M.A.K.L. Dissanayake<sup>b,\*</sup>, G.K.R. Senadeera<sup>b,c</sup>

<sup>a</sup> Department of Physics, University of Peradeniya, Peradeniya, Sri Lanka

<sup>b</sup> National Institute of Fundamental Studies, Kandy, Sri Lanka

<sup>c</sup> Department of Physics, The Open University of Sri Lanka, Nawala, Nugegoda, Sri Lanka

## ARTICLE INFO

### Article history:

Received 8 May 2018

Received in revised form

9 December 2018

Accepted 15 December 2018

Available online 18 December 2018

### Keywords:

Dye sensitized solar cells

Efficiency enhancement

Silver nanowires

Plasmonic effect

Tri-layered photoanode

TiO<sub>2</sub> nanofibers

## ABSTRACT

The effect of incorporating silver nanowires (Ag NWs) and TiO<sub>2</sub> nanofibers (NFs) into a tri-layer photoanode of dye sensitized solar cells (DSSCs) have been investigated. Ag NWs with diameter 60–90 nm and length of 1–2 μm were synthesized via polyol reduction method. TiO<sub>2</sub> nanofibers (NFs) with diameter 80–120 nm were prepared by electrospinning. The DSSC with tri-layer photoanode made with a composite of TiO<sub>2</sub> P25, Ag NWs and TiO<sub>2</sub> NFs sandwiched between two TiO<sub>2</sub> P25 layers exhibited power conversion efficiency of 9.74% and open circuit voltage ( $V_{oc}$ ), short circuit current density ( $J_{sc}$ ) and fill factor ( $FF$ ) of 727.4 mV, 19.8 mA cm<sup>-2</sup> and 67.6% respectively under the irradiance of 100 mW cm<sup>-2</sup>. The efficiency of the reference DSSC with TiO<sub>2</sub> P25/P25/P25 tri-layer photoanode of the same thickness was found to be 6.69%. The efficiency enhancement of the DSSC with Ag NWs and TiO<sub>2</sub> NF incorporated composite, tri-layer photoanode compared to the reference DSSC is 45.6%. This is evidently due to the enhancement in short-circuit photocurrent density ( $J_{sc}$ ) by (a) localized surface plasmon resonance effect by Ag NWs and (b) increased light harvesting by multiple scattering events by the presence of TiO<sub>2</sub> NFs.

© 2018 Elsevier Ltd. All rights reserved.

## 1. Introduction

The conventional DSSC is a device generally consisting of a mesoporous layer of TiO<sub>2</sub> nanoparticles with a monolayer of Ruthenium dye adsorbed on the TiO<sub>2</sub> nanoparticle surfaces, a liquid or quasi-solid (gel) electrolyte with iodide/triiodide redox couple and a platinized counter electrode. Since the first report of the DSSC by Gratzel et al., in 1991 [1], it is under intense research in order to develop low cost, stable and high performance solar cells. These were mainly achieved by developing better photoanodes [2–4], novel sensitizers [5–8] and novel electrolytes [9–15].

The dye adsorbed photoanode is one of the key components of a DSSC which determines its efficiency. The efficiency of a DSSC can be substantially enhanced either by increasing the thickness of the photoanode and hence by increasing the dye adsorption or fabricating photoanodes with suitable structural modifications [2–4].

However, increase of the film thickness is not that simple due to various reasons such as poor adherence to the substrate, formation of cracks, reduction of light penetration etc. Therefore, most of the recent research studies have been focused on the structural modifications of the photoanode in order to increase light absorption. These have been achieved, for example, by incorporation of TiO<sub>2</sub> nanofibers (NFs), Nanotubes, Nano wires (NWs) or Nano flakes into the photoanode [13–19].

Light trapping or scattering techniques can also be used effectively to improve the performance of the photoanodes which could enhanced the short circuit photocurrent and hence the efficiency of a DSSC. Strategically designed and nanostructurally developed, smart light trapping techniques can be used to obtain 'optically thick' light absorbers to allow substantially enhanced light absorption [20]. Generally this light trapping or scattering is achieved by using a scattering layer with bigger size nanoparticle layer (~300–700 nm) deposited on top of a smaller size nano particle (~20 nm) layer [21,22].

Recently, it has also been explored that, incorporating TiO<sub>2</sub>

\* Corresponding author.

E-mail address: [makldis@yahoo.com](mailto:makldis@yahoo.com) (M.A.K.L. Dissanayake).

nanofibers (NFs) to the photoanode is another way to increase the optical thickness of the photoanode.  $\text{TiO}_2$  NFs can trap more light by scattering the incoming light. Mie scattering theory successfully explains the light scattering by  $\text{TiO}_2$  NFs [23]. Here the “optical thickness” of the photoanode is increased due to the tailoring of the photoanode composition and the geometry either by using NFs or Nanowires (NWs) in the structure of the photoanode [24–33]. In order to further enhance the overall performance of DSSCs, strategically increasing the short circuit photocurrent density by nanostructural modifications to the photoanode could be implemented. By tailoring the photoanode composition, and geometry with 1-D nanostructures such as  $\text{TiO}_2$  NWs and  $\text{TiO}_2$  NFs, improvements in electron mobility and transport have been observed [34–37].

In recent DSSC studies, it has also been observed that localized surface plasmon resonance (LSPR) effect by metallic nanostructures can be successfully utilized for efficiency enhancement [38]. When an electromagnetic (EM) wave is incident on a metal surface, due to the electric field component of EM wave, there will be collective oscillations of the surface conduction electrons or surface plasmons. As metal nanostructures have sub wavelength dimensions, oscillation of electron cloud (plasma) is localized/confined around the surface of the nanostructure resulting LSPR effect. There are mainly four light enhancement types contributing to generation of photoelectrons via LSPR effect in DSSC photoanodes; (1) near field coupling of electromagnetic fields, (2) far-field coupling of scattered light (3) plasmon resonance energy transfer and (4) hot electron transfer [39–43]. Silver is a noble metal showing strong LSPR effects [43,44]. Thus, by incorporating Ag NWs to photoanode of a DSSC, an enhancement in DSSC performance originating from the increase in the photocurrent has been achieved [44–47].

In the present study, DSSCs made with four types of tri-layered  $\text{TiO}_2$  photoanodes consisting of a composite mixture made of  $\text{TiO}_2$  nano-particles (NP),  $\text{TiO}_2$  nanofibres (NFs) and Ag nanowires (NWs) and sandwiched between two  $\text{TiO}_2$  NP layers were fabricated and characterized. A liquid phase bottom-up polyol reduction synthesis method was used to chemically synthesis Ag NWs while the electrospinning method was used to fabricate  $\text{TiO}_2$  NFs. To the best of our knowledge, this is the first report of the use of a tri-layer  $\text{TiO}_2$  photoanode structure consisting of a composite middle layer of  $\text{TiO}_2$  P25 nanoparticles,  $\text{TiO}_2$  nanofibres and Ag nano wires in a DSSC aiming at maximizing the light harvesting efficiency.

## 2. Experimental

### 2.1. Synthesis of silver nanowires (Ag NWs)

#### 2.1.1. Materials

For the synthesis of Ag NWs, silver nitrate ( $\text{AgNO}_3$ , 99.8%, Daejung), polyvinyl pyrrolidone (PVP, Mw = 44,000, BOH Laboratories), glycerol (Surechem Products LTD), sodium chloride ( $\text{NaCl}$ , 99.5%, Sigma-Aldrich) were used as received without any further purification. The deionized (DI) water was used from the Millipore system.

#### 2.1.2. Synthesis of Ag NWs

The Ag NWs were synthesized using polyol reduction process published elsewhere [44]. First, 47.5 ml of glycerol and then 1.500 g of PVP were added to a round bottom flask. Then, the solution was gently heated up to 80 °C until all PVP was dissolved. The solution was then allowed to cool down to room temperature and 0.395 g of  $\text{AgNO}_3$  powder was added to the solution. Subsequently, 0.125 ml of  $\text{NaCl}$  solution (5 mmol/L) was added to 2.5 ml of glycerol and the latter was added to the PVP dissolved solution containing  $\text{AgNO}_3$  powder. Next, the reaction temperature of the solution was

increased rapidly to 210 °C, roughly at a rate of 8 °C per min. while stirring in a magnetic stirrer at 50 rpm under aerobic condition. When the temperature reached 210 °C the heating was stopped and the solution was allowed to cool down to room temperature. Then 50 ml of DI water was added to the flask and the mixture was centrifuged at 8000 rpm for 20 min and Ag NWs were collected. Finally, in order to remove the residues including PVP, nano wires were washed with copious amount of DI water by centrifuging the suspension.

#### 2.1.3. Characterization of Ag NWs

In order to study the optical properties of the synthesized Ag NWs, a suspension of nanowires was prepared with DI water and UV–visible absorption spectrum was obtained using a Shimadzu UV-1800 spectrometer. The dimensions and the morphology of the Ag NWs were studied using a scanning electron microscope (SEM, EVO LS15).

### 2.2. Synthesis of $\text{TiO}_2$ NFs

#### 2.2.1. Materials

Poly (vinyl acetate) (PVA,  $(\text{C}_4\text{H}_6\text{O}_2)_n$ ), titanium isopropoxide (TIP,  $\text{C}_{12}\text{H}_{28}\text{O}_4\text{Ti}$ , Fluka Chemie, Switzerland) and acetic acid (99%, Fisher), N,N-dimethylformamide (DMF, Degussa) were used as starting materials to synthesize  $\text{TiO}_2$  NFs.

#### 2.2.2. Preparation of $\text{TiO}_2$ NFs

A mixture containing 1.5 g of PVA, 3 g of titanium (iv) isopropoxide (TIP) and 1.2 g of acetic acid as a catalyst for sol-gel reaction in 19 ml of DMF was magnetically stirred for 6 h. Then, the solution was electrospun to obtain  $\text{TiO}_2$  nanofibres (NF) under a voltage of 15 kV applied between the syringe needle tip and the grounded drum collector. The distance between the nozzle and collector was kept at 6.5 cm. The drum was rotated with a rotational speed of 650 rpm. The electrospun  $\text{TiO}_2$  NFs were deposited on pre-cleaned glass plates. Finally, the electrospun NFs were calcined at 450 °C for 45 min.

#### 2.2.3. Characterization of $\text{TiO}_2$ NFs

The dimensions and the morphology of the Ag NWs were studied using a scanning electron microscope (SEM, EVO LS15).

### 2.3. Fabrication of DSSC

#### 2.3.1. Fabrication of pristine $\text{TiO}_2$ nanoparticle ( $\text{TiO}_2$ -NP) photoanode

In one of our previous studies, we have optimized the film thickness of the  $\text{TiO}_2$  nanoparticle layer suitable for DSSCs [37]. However in that study we have fabricated the  $\text{TiO}_2$  nanoparticle films as a single layer and the DSSC with highest efficiency was obtained with a ~12.73  $\mu\text{m}$  thick  $\text{TiO}_2$  film. Further increase of the thickness of the  $\text{TiO}_2$  film resulted in a decrease of the efficiency of the DSSC and it was difficult to fabricate thicker films due to poor adherence to Fluorine doped tin oxide glass substrate (FTO) substrate. Therefore, by considering these factors, in this study, we have fabricated thicker photoanodes by sequentially forming the three layered photo anodes with pristine  $\text{TiO}_2$  nanoparticles (P25NPs) with optimized total thickness of about 28  $\mu\text{m}$ . Further improvements in the adherence and the reduction of short-circuiting were achieved by applying a pinhole free compact layer (CL) on the FTO substrate [47].

At first, a paste was prepared by grinding 0.250 g  $\text{TiO}_2$  (Aeroxide P-90) with 1.0 ml of 0.1 M  $\text{HNO}_3$  for 15 min. The paste was then spin coated on pre-cleaned FTO glass substrate (Solaronix sheet glass 7  $\Omega/\text{sq}$ ) at 3000 rpm for 60 s, followed by sintering at 450 °C for

45 min to obtain a compact layer (CL) on the FTO substrate. After cooled down to room temperature, on top of the compact layer, a single layer of mesoporous TiO<sub>2</sub> was deposited as follows. First, 0.250 g of TiO<sub>2</sub> powder (Desgussa P-25) was ground for 30 min with 1.0 ml of 0.1 M HNO<sub>3</sub>, one drop of Triton X-100 and 0.050 g of polyethylene glycol (PEG). The paste was then spread on top of the compact layer by “doctor blading” method, followed by sintering at 450 °C for 45 min to obtain the first TiO<sub>2</sub> nanoparticle (NP) layer on the compact layer. After cooling down to room temperature another layer of TiO<sub>2</sub> (P25NP) was deposited on top of the above layer and sintered by following the same procedure. Finally a third layer of P25 NP was applied on top of the above double layered structure by following the same procedure. After cooled down to room temperature, these glass substrates with tri-layered TiO<sub>2</sub> NP films were dipped in an ethanolic dye (0.3 mM) solution containing Ruthenium dye N719 [RuL2 (NCS)2:2TBA where, L = 2,2'-bipyridyl-4,4'-dicarboxylic acid TBA = tetrabutylammonium] for 24 h. The effective area of the photoanodes was kept as 0.25 cm<sup>2</sup>. The total film thickness of the tri-layer TiO<sub>2</sub> photoanode, estimated from SEM analysis was ~28 μm. In order to compare the efficiencies of DSSCs, dye adsorption was also carried out for a single layered (~12.73 μm) TiO<sub>2</sub> NPs photoanode as in the other cases.

### 2.3.2. Preparation of Ag NWs incorporated photoanodes

In order to find the optimum composition ratio of TiO<sub>2</sub> P25 to Ag NWs, which gives the highest DSSC efficiency, a single layer, conventional type photoanode was fabricated with configuration, FTO/P90/(P25NP + AgNW) as described previously [47]. A series of DSSCs were fabricated by varying the Ag NW wt% added to P25NP in the photoanode from 0.0 to 2.6 wt%. The DSSC with 2.2 wt% of Ag NWs in the composite photoanode exhibited the highest power conversion efficiency. This optimized ratio was maintained for the fabrication of the middle composite layer in the two tri-layer photoanodes (c) (P25NP + Ag NW) and (d) (P25NP + TiO<sub>2</sub>NF + Ag NW) described later. Appropriate amount of AgNWs were added to the TiO<sub>2</sub> paste (either P25 OR P25 + NF) prepared for the doctor blade method and ground well the mixture and films were spread by doctor blade method. TiO<sub>2</sub> photoanodes incorporating Ag NWs were heat treated at 450 °C for 45 min. After cooled down to room temperature dye adsorption was carried out as described previously.

### 2.3.3. Preparation of TiO<sub>2</sub> NFs incorporated photoanodes

Similar to optimization of photoanode composition by incorporating Ag NWs [47], DSSCs having different amounts of TiO<sub>2</sub> NFs in their photoanodes were fabricated. The optimized DSSC efficiency was achieved by mixing 95% TiO<sub>2</sub> (P 25) powder (0.2375 g) with 5% electrospun TiO<sub>2</sub> NF powder (0.0125 g).

### 2.3.4. Preparation of the redox electrolyte

The redox electrolyte solution containing I<sup>-</sup>/I<sub>3</sub><sup>-</sup> was prepared by adding a 3.6 ml of molten ethylene carbonate (EC) and 1.0 ml of acetonitrile to a pre-cleaned 10 ml volumetric flask. Then the solution was stirred overnight, after adding a 0.738 g of tetrapropyl ammonium iodide (Pr<sub>4</sub>NI) and 0.060 g of I<sub>2</sub> to the volumetric flask.

### 2.3.5. Fabrication of solar cells and their I-V characterization

DSSCs were fabricated using four different types of tri-layer TiO<sub>2</sub> photoanodes as described below. When preparing these four photoanodes, the total thickness (of the three layers) was kept nearly constant around 28 μm while the thickness of each layer was in the 8–10 μm range (one scotch tape). For all four types of photoanodes, the FTO/P90 (compact layer) and P25 TiO<sub>2</sub> first layer was prepared identically. The labeling of the four types of photoanodes are: (a) FTO/P90/P25NP/**P25NP**/P25NP tri-layer where the middle

layer consists of P25NP, (b) FTO/P90/P25NP/(**P25NP + TiO<sub>2</sub> NF**)/P25NP, where the middle layer consists of the optimized, composite mixture of P25NP and TiO<sub>2</sub>NF, (c) FTO/P90/P25NP/(**P25NP + Ag NWs**)/P25NP, where the middle layer consists of the optimized composite mixture of P25NP and AgNWs and (d) FTO/P90/P25NP/(**P25 + TiO<sub>2</sub> NFs + Ag NWs**)/P25NP, where the middle layer consists of the optimized composite mixture of P25NP, TiO<sub>2</sub> NFs and Ag NWs.

In the above labeling, the middle layer is indicated by bold letters in the four photoanodes for clarity. For each tri-layer photoanode, a DSSC with a single layer photoanode was used to optimize the composition ratio of TiO<sub>2</sub>P25NP, TiO<sub>2</sub> NF and AgNW) by measuring the performance of test DSSCs. The best composition ratio was then used to fabricate the middle layer of the tri-layer photoanode for all subsequent studies.

In order to compare the performances of DSSCs four different types of solar cells consisting of dye adsorbed tri-layer photoanodes, were prepared by sandwiching each of them with Pt coated FTO glass counter electrodes together with the above electrolyte. The total thickness of each of the above (a), (b), (c) and (d) photoanodes were kept nearly the same at ~28 μm.

The photocurrent-voltage (I-V) characteristics of the prepared DSSCs were measured under the simulated sunlight illuminating at 100 mW cm<sup>-2</sup> (AM 1.5). A Xenon 500 W lamp with AM 1.5 filter was used as the solar simulator to obtain the above intensity. The solar simulator was coupled to a Keithley 2000 multimeter and a potentiostat/galvanostat HA-301.

### 2.3.6. Incident photon to current efficiency (IPCE) measurements

IPCE measurements were taken for the above four DSSCs fabricated with the four different types of tri-layer photoanodes, (a), (b), (c) and (d). Experimental setup consisted of monochromatic light illumination from a Bentham PVE300 unit equipped with a TMC 300 monochromator-based IPCE system. 150 W xenon arc lamp was used to obtain monochromatic light in the wavelength range of 300–800 nm. A calibrated Si photo detector (type DH) as used as the reference cell.

### 2.3.7. Electrochemical impedance Spectroscopy (EIS) measurements on DSSCs

EIS measurements were performed on the above four DSSCs using a Metrohm Autolab Potentiostat/Galvanostat PGSTAT 128 N with a FRA 32 M Frequency Response Analyzer (FRA) covering the 1 MHz to 0.01 Hz frequency range. These measurements were carried out under the illumination of 100 mW cm<sup>-2</sup> (AM 1.5) simulated sunlight using the same solar simulator that was used for I-V measurements.

## 3. Results and discussion

### 3.1. Single layer DSSC

Fig. 1 shows the SEM image of the cross section of the mesoporous single layer TiO<sub>2</sub> (P25NP) photoanode incorporating Ag NWs. It should be mentioned here that single layer TiO<sub>2</sub> films of larger thickness than what is shown in Fig. 1 could not be formed by the doctor blade method due to poor adhesion to the FTO substrate and due to cracking during sintering. Whether it is pure TiO<sub>2</sub> (P25NP) or a mixture of P25 NP with TiO<sub>2</sub> NF or Ag NW, 12.73 μm is about the maximum film thickness that could be formed on a single run without cracking [37,47]. However, we found that thicker, crack-free TiO<sub>2</sub> photoanode films could be formed by doctor blading followed by sintering layer by layer. Therefore, in this study, layer by layer fabrication and sintering technique was used to obtain a thicker, crack-free TiO<sub>2</sub> P25NP/**P25NP**/P25NP tri-layer

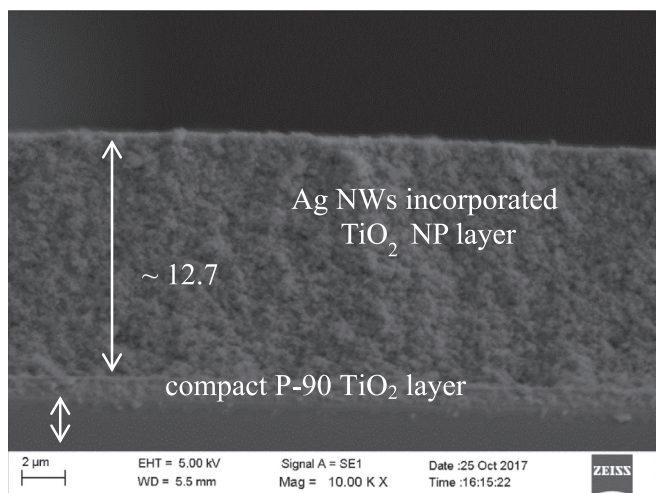


**Fig. 1.** Cross sectional SEM image of the Ag NWs incorporated single-layered TiO<sub>2</sub> photoanode.

photoanodes on compact P90 TiO<sub>2</sub> layer. The same layer by layer, sequential procedure was followed for the fabrication of other three tri-layer photoanodes, (b), (c) and (d).

SEM images of the top view of the synthesized Ag NWs and electrospun TiO<sub>2</sub> NFs are shown in Fig. 2. As seen from these images, the average dimensions of the synthesized Ag NWs are ~2.5 μm in length and ~78 nm in diameter. The average diameter of the TiO<sub>2</sub> NFs is about 115 nm.

### 3.2. DSSCs with tri-layer photoanodes

As mentioned previously, since it was not possible to make a thicker, single layer TiO<sub>2</sub> anode in a single run due to poor adherence to the FTO and cracking problems, here we have used a layer by layer depositing and sintering at a time to fabricate a thicker TiO<sub>2</sub> photoanode. SEM image in Fig. 3 shows that the total thickness of the optimized tri-layer photoanode is ~28 μm and the thickness of each TiO<sub>2</sub> layer is around 8.00–10.00 μm. The optimized total film thickness of the tri-layer TiO<sub>2</sub> photoanode used in each DSSC was found to be about 28 μm. Having a thicker, tri-layer, pristine TiO<sub>2</sub> photoanode (P25NP/P25NP/P25NP) as the reference is useful when the effects of different middle layers on the photovoltaic performances of DSSCs are studied.

One of the SEM images of the tri-layered photoanode, (d) FTO/P90/P25NP/(P25NP + Ag NWs + TiO<sub>2</sub> NF)/P25NP, is presented in Fig. 3 as a representative example. In other two SEM images (not

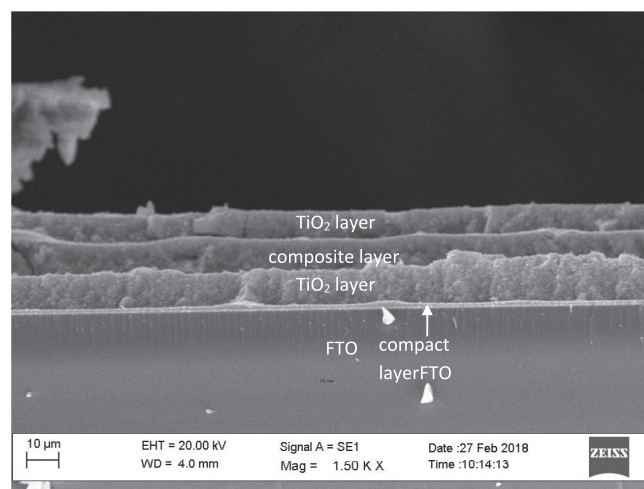


**Fig. 3.** SEM image of TiO<sub>2</sub> photoanode of the tri-layered structure, (d) P25NP/P25NP + TiO<sub>2</sub> NF + Ag NWs + P25NP formed on FTO/P90 compact layer correspond to the DSSC showing the best photovoltaic performance. The composite middle layer consists of the optimized composition of P25NP + TiO<sub>2</sub> NF + Ag NWs.

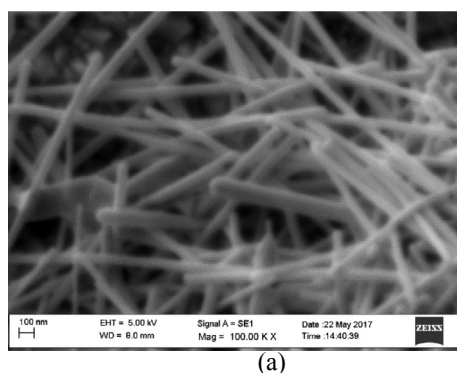
shown), the composite middle layer appears similar but consists of one of the compositions, (P25NP + TiO<sub>2</sub>NF) or (P25NP + Ag NWs) in optimized composition ratios. Fig. 4 shows the schematic diagram of the DSSC made with the above tri-layer photoanode (d).

#### 3.2.1. Photovoltaic performance

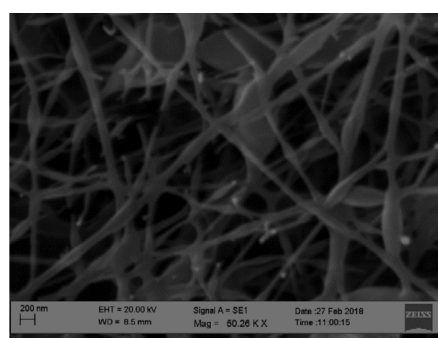
The photovoltaic performance of the DSSCs with above four different types of tri-layered photoanodes measured under the simulated sunlight illuminating at 100 mW cm<sup>-2</sup> (AM 1.5) are shown as *J-V* curves in Fig. 5.

The corresponding photovoltaic parameters derived from above figure are tabulated in Table 1.

From a comparison of the performance of the DSSCs fabricated with four different composite, three layered photoanodes (a), (b), (c) and (d) shown in Fig. 5 and Table 1, the results of improved short circuit photocurrent and the enhanced efficiency with modified photoanodes can be interpreted as follows. The increased photocurrent density and the efficiency when the TiO<sub>2</sub> P25 middle layer is replaced by a mixture of TiO<sub>2</sub> P25 NP and TiO<sub>2</sub> NF (from photoanode (a) to photoanode (b)), is evidently due to the improved light harvesting due to presence of the TiO<sub>2</sub> nanofibres in the middle layer. This is very likely due to the increased light absorption caused by multiple scattering effects within the TiO<sub>2</sub> nanofibre based photoanode as already reported by us and by others [23–37]. As a



(a)



(b)

**Fig. 2.** SEM images of (a) synthesized Ag NWs and (b) electrospun TiO<sub>2</sub> NFs used in this work.

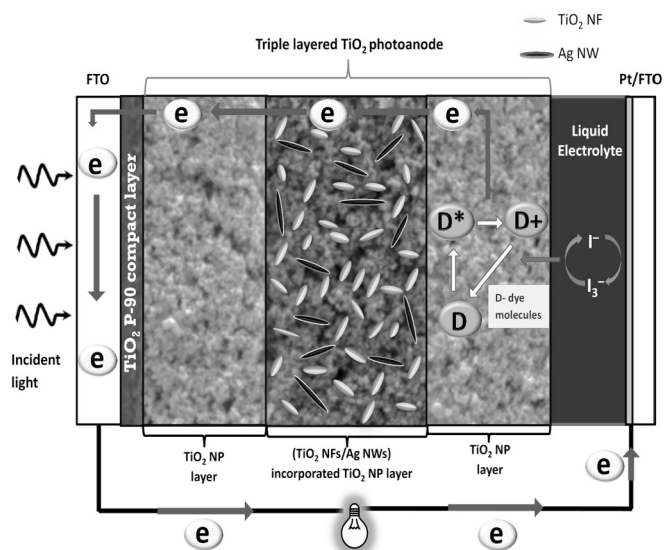


**Fig. 4.** A schematic diagram of the DSSC with the tri-layer photoanode with the configuration of P25NP/P25NP + TiO<sub>2</sub> NF + Ag NW/P25NP. The middle region of this tri-layered photoanode structure shows the composite mixture of P25NP TiO<sub>2</sub> with TiO<sub>2</sub> NFs and Ag NWs.

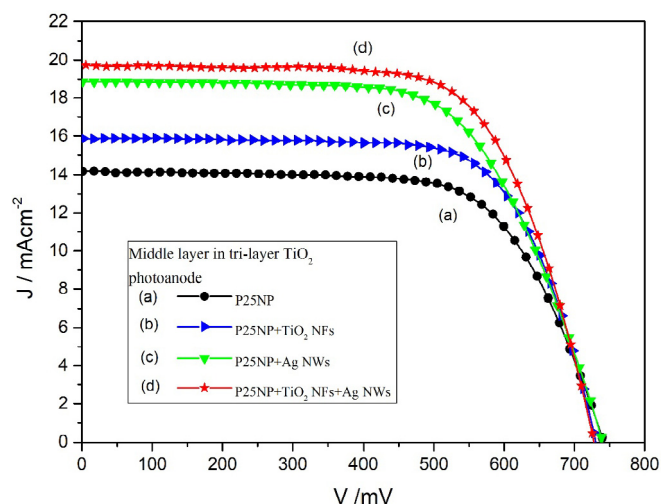


**Fig. 5.** Current density –voltage ( $J$ - $V$ ) curves of DSSCs fabricated with four typed of tri-layer photo anodes: (a) FTO/P90/(P25NP)/P25NP/P25NP (b) FTO/P90/(P25NP + TiO<sub>2</sub>NF)/P25NP, (c) FTO/P90/P25NP/(P25NP + Ag NWs)/P25NP and (d) FTO/P90/P25NP/(P25 + TiO<sub>2</sub>NFs + AgNWs)/P25NP.

result, the  $J_{sc}$  has increased by 10.5% and the efficiency by 20.6%. In previous papers we have described in detail, somewhat qualitatively, how multiple light scattering events contribute to the enhancement of light harvesting within the TiO<sub>2</sub> nanofibre structure consisting of “elongated bead” shaped short nanofibers formed

after sintering [26,27]. Multiple scattering events by elongated nanofibre beads within the sintered NF layer coupled with possible back and forth reflections from the two interfaces on either side of middle layer of the TiO<sub>2</sub> photoanode appears to contribute to this enhancement.

Zhu et al. has reported that the efficiency enhancement in their DSSCs made with “rice grain shaped” TiO<sub>2</sub> nanobeads is due to improved light harvesting by scattering [24]. Similar improvement in light harvesting by scattering by a composite TiO<sub>2</sub> electrode consisting of a mixture of electrospun TiO<sub>2</sub> nanofibres and conventional TiO<sub>2</sub> nanoparticles has been discussed in detail by Joshi et al. [25]. These authors have attributed the enhancement in efficiency to the enhanced photocurrent due to improved light harvesting through Mie scattering. According to their results, under the same fabrication conditions and with the same TiO<sub>2</sub> photoanode film thickness, the DSSCs made from the composite with 85 wt% nanoparticles and 15 wt % nanofibers have showed a 44% higher efficiency compared to those made from TiO<sub>2</sub> nanoparticles alone. Through a modelling study, these authors have further established that the forward scattering has increased strongly with increasing nanofiber diameter (200 nm and up) while the backward scattering was negligible regardless of fiber diameter. The intensity of the forward scattering for the nanofibers with diameters less than 200 nm was relatively weak. In our work also, the increase in  $J_{sc}$  of the DSSC with TiO<sub>2</sub> NP + NF composite very likely results from a similar improved light harvesting caused by scattering by the TiO<sub>2</sub> elongated bead like structure. In our case, the diameter of the NF beads are around 115 nm. These beads, are very likely randomly distributed within the middle TiO<sub>2</sub> composite layer in the photoanode, and scatter incident light effectively resulting in a substantial increase in light absorption within the layer and also by the two adjacent TiO<sub>2</sub> NP layers. In line with the already published reports listed above, we can infer that the enhancement in the photocurrent and the efficiency of the DSSCs with tri-layer photoanode (b) P25NP/(P25NP + TiO<sub>2</sub> NF)/P25NP where the middle layer consists of a mixture of TiO<sub>2</sub> nanoparticles (95 wt%) and TiO<sub>2</sub> nanofibres (5 wt%) used in our work is evidently due to the scattering enhanced photocurrent due to the presence of the optimized nanoparticle-nanofibre (“elongated beads”) composite middle layer sandwiched between the two TiO<sub>2</sub> P25NP layers.

According to Jeong et al., silver nanoparticles photochemically incorporated into a TiO<sub>2</sub> nanoparticulate framework in a DSSC photoanode have shown a significantly higher wavelength-dependent IPCE spectrum across the visible spectrum and the integrated IPCE values were found to be similar to the increase in  $J_{sc}$  values compared to the silver nanoparticle free photoanode [52]. The IPCE increase was attributed to the improved light harvesting manifested mainly as photocurrent density increase by surface plasmon resonance effect by Ag nanoparticles. Chandrasekhar et al. [53] have shown that when 0.9 wt % of Ag nanowires are incorporated into the mesoporous TiO<sub>2</sub> photoanode in a DSSC, the photocurrent density and the efficiency have increased significantly due to increased light absorption. This has been ascribed to the improvement in light harvesting by LSPR effect by Ag nanowires.

**Table 1**  
Photovoltaic parameters of the DSSCs with tri-layer photoanodes: (a) FTO/P90/(P25NP)/P25NP/P25NP (b) FTO/P90/P25NP/(P25NP + TiO<sub>2</sub>NF)/P25NP, (c) FTO/P90/P25NP/(P25NP + Ag NWs)/P25NP and (d) FTO/P90/P25NP/(P25 + TiO<sub>2</sub>NFs + AgNWs)/P25NP.

Tri-layered photoanode configuration formed on FTO/P90 compact layer	$J_{sc}$ (mAcm <sup>-2</sup> )	$V_{oc}$ (mV)	FF (%)	$\eta$ (%)
(a) P25NP/(P25NP)/P25NP (reference)	14.3	746.9	62.6	6.69
(b) P25NP/(P25NP + TiO <sub>2</sub> NF)/P25NP	15.8	729.7	70.0	8.07
(c) P25NP/(P25NP + Ag NW)/P25NP	18.9	741.9	62.7	8.94
(d) P25NP/(P25NP + TiO <sub>2</sub> NF + Ag NW)/P25NP	19.8	727.4	67.6	9.74

In the case of metal nanostructures, the radiative and non-radiative plasmonic properties are controlled to a large extent by their dimension, which strongly influence their light harvesting capability. In this context, it is generally established that while nanostructures < 90 nm in diameter are strong absorbers, nanostructures > 90 nm primarily contribute to scattering [54]. As seen from the SEM images (Fig. 2), the average dimensions of the synthesized Ag NWs are ~2.5  $\mu\text{m}$  in length and ~78 nm in diameter suggesting that these NWs will strongly absorb visible light by surface plasmon resonance effect.

As explained in several papers mentioned in the introduction section, the localized surface plasmon resonance (LSPR) effect is very likely responsible for the observed enhancement in the photocurrent and the efficiency in the DSSCs with tri-layer photoanode, (c) P25NP/(P25NP + Ag NW)/P25NP where the middle layer consists of the optimized mixture of TiO<sub>2</sub> P25NP and Ag NWs [38–47,52–54]. The increase in  $J_{sc}$  and efficiency is more prominent here compared to the photoanode (b) made with TiO<sub>2</sub> NFs in the middle layer. The photocurrent density has increased by 32% and the efficiency by 33.6% with respect to the pristine photoanode (a) P25NP/P25NP/P25NP.

When the middle layer is replaced by the optimized composite mixture of TiO<sub>2</sub> P25NP powder, sintered electrospun TiO<sub>2</sub> nanofibres (TiO<sub>2</sub> NF) and silver nanowires (Ag NWs), i.e. when the photoanode structure is changed from (a) P25NP/(P25NP)/P25NP to (d) P25NP/(P25NP + TiO<sub>2</sub> NF + Ag NW)/P25NP, the increase in  $J_{sc}$  and efficiency is much more dramatic. The photocurrent density has increased by 38.5% and the overall efficiency by 45.6% with respect to the basic (reference) DSSC with pristine P25NP/P25NP/P25NP trilayer photoanode of the same total thickness. The cumulative effect of both, “scattering enhanced photocurrent” due to TiO<sub>2</sub> NFs as well as the “plasmon enhanced photocurrent” due to Ag NWs are evidently responsible for this remarkable photocurrent and efficiency enhancement. To the best of our knowledge, the use of a tri-layer TiO<sub>2</sub> photoanode structure consisting of a composite of TiO<sub>2</sub> P25 nanoparticles, TiO<sub>2</sub> Nanofibres and Ag nano wires to achieve a high efficiency enhancement in a DSSC has not been reported so far.

### 3.2.2. IPCE analysis

IPCE measurements on DSSCs reflect the effectiveness of converting incident light photons to electrons at different incident wavelengths. The IPCE values taken as a function of wavelength for the DSSCs with the four different types of tri-layer TiO<sub>2</sub> photoanodes, (a) P25/(P25)/P25, (b) P25/(P25 + TiO<sub>2</sub>NF)/P25, (c) P25/(P25 + AgNW)/P25 and (d) P25/(P25 + TiO<sub>2</sub> NF + Ag NWs)/P25 are shown in Fig. 6.

As depicted in Fig. 6 by curves (a) and (b), the DSSC fabricated with a tri-layer TiO<sub>2</sub> photoanode (b) comprising a mixture of TiO<sub>2</sub> P25 and TiO<sub>2</sub> nano fibres (NF) in the middle layer shows a higher IPCE value than the DSSCs fabricated with photoanode (a) with TiO<sub>2</sub> P25 as the middle layer. This is consistent with the photocurrent densities and efficiencies exhibited by DSSCs fabricated with these two photoanodes (Fig. 5). This enhancement in IPCE can be attributed to the increased photocurrent density due to increased light absorption by scattering events within the dyed TiO<sub>2</sub> nanofibre (elongated TiO<sub>2</sub> beads) network. Similar observations have been made by Shalan et al. [51] for DSSCs made with photoanodes fabricated with TiO<sub>2</sub> nanorods.

Comparison of IPCE curves (a) and (c) shows effect of Ag NWs (silver nanowires) in the middle layer in photoanode (c). The presence of AgNWs has made a remarkable increase in the IPCE values as well as widen the wavelength range of photon absorption. The increase in integrated area under curve (c), which is sufficiently large in comparison with curve (a), would correspond to the

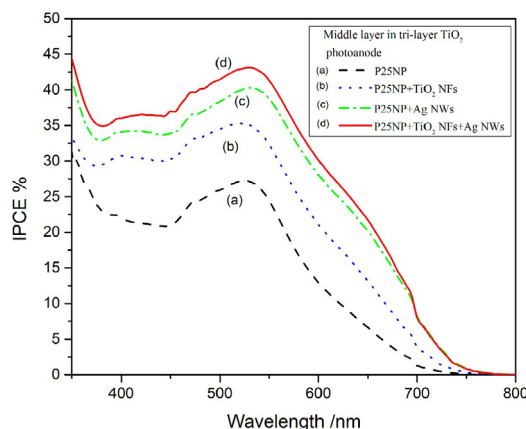


Fig. 6. IPCE spectra of DSSCs fabricated with four different photoanodes (a) P25/(P25)/P25, (b) P25/(P25 + TiO<sub>2</sub> NF)/P25, (c) P25/(P25 + Ag NW)/P25 and (d) P25/(P25 + TiO<sub>2</sub> NF + Ag NWs)/P25.

increase in short circuit current density in the DSSC made with photoanode (c). This increase is evidently caused by the local surface plasmon resonance effect by AgNWs as explained later.

Comparison of IPCE curves (a) and (d) shows that both the IPCE values as well as the wavelength range covered have increased much more dramatically due to the incorporation of both TiO<sub>2</sub> NFs as well as AgNWs into the middle layer of the photoanode (d). This remarkable increase can evidently be attributed to both, scattering enhanced light absorption by the presence of TiO<sub>2</sub> NF nanofibres as already described, as well as the increased optical absorption due to surface plasmon resonance effect by Ag NWs.

A considerable number of papers can be cited where the IPCE spectra has been used convincingly to demonstrate the LSPR effect by silver nanostructures in enhancing the photocurrent and the efficiency of DSSCs [38–47,52–54]. Further, the broadening and the red shifting of the IPCE spectrum of the DSSC with AgNWs incorporated photoanodes seen in Fig. 6 further confirms the effect of AgNWs in the photoanode as these are some characteristics of the Ag nanoparticles [52]. As the photocurrent enhancement (Fig. 5 and Table 1) and the enhancement in the IPCE spectrum (Fig. 6) are obtained from two independent experiments they provide sufficient evidence for the efficient light usage to generate photoelectrons via surface plasmon resonance effect by Ag nanowires. The highest IPCE values (curve (d)) among all the DSSCs tested in this work results from the combined effect of both the enhanced light absorption by scattering by TiO<sub>2</sub> NFs and the enhanced photocurrent via surface plasmon resonance effect by Ag NWs.

### 3.2.3. EIS analysis

Electrochemical impedance spectroscopy was performed in order to understand the electronic and ionic processes in DSSCs [48]. We have limited these measurements only to the DSSCs made with tri-layer photoanodes (a) and (d) in order to better focus on the results and to improve the clarity of presentation. Nyquist plots and the Bode Plots in the frequency range from  $11 \times 10^{-2}$  to  $11 \times 10^6$  Hz taken for the DSSCs with photoanode configurations (on FTO/TiO<sub>2</sub> compact layer) (a) P25/P25/P25 and (d) (P25/P25 + TiO<sub>2</sub> NF + Ag NWs/P25) are shown in Figs. 7 and 8 respectively. The corresponding parameters extracted from the equivalent circuit analysis and Bode plots are tabulated in Table 2.

In each Nyquist plot, the larger semicircle in the low frequency

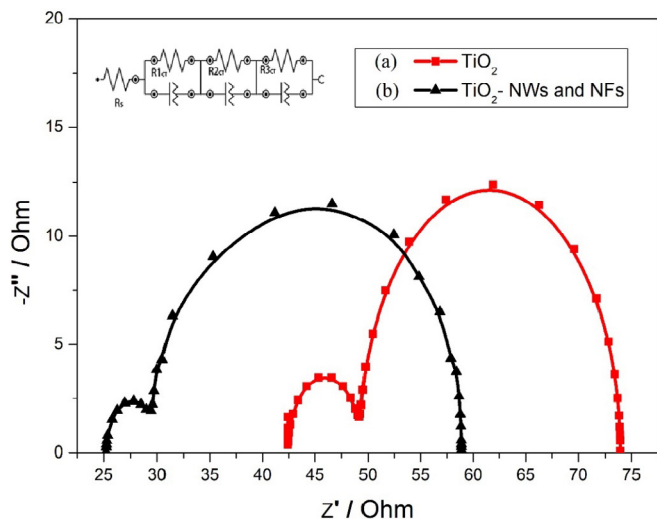


**Fig. 7.** Impedance plots taken for the DSSCs with tri-layer photoanodes (a) (P25/P25/P25) and (d) (P25/P25 + TiO<sub>2</sub> NF + Ag NWs/P25) in the frequency range from  $11 \times 10^{-2}$  to  $11 \times 10^6$  Hz.

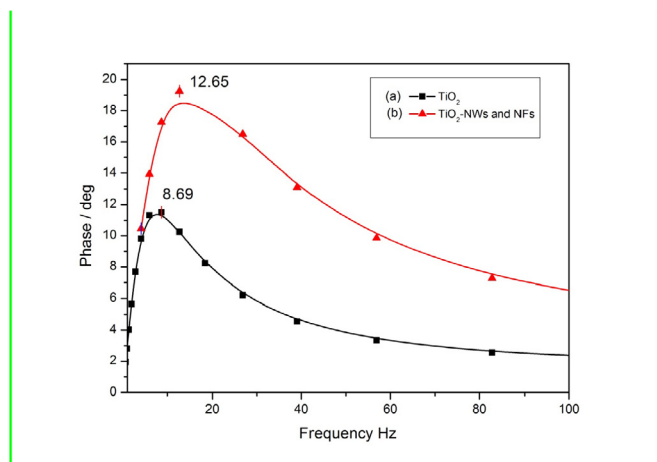


**Fig. 8.** Bode phase plots taken for the DSSCs with photoanodes (a) (P25/P25/P25) and (b) (P25/P25 + TiO<sub>2</sub> NF + Ag NWs/P25) in the frequency range  $11 \times 10^{-2}$  to  $11 \times 10^6$  Hz.

range corresponds to the charge transport/accumulation at dye-attached TiO<sub>2</sub>/electrolyte interface with resistance ( $R_{2CT}$ ) and the smaller semicircle in the high frequency range corresponds to the charge-transfer resistance of the Pt counter electrode/electrolyte interface ( $R_{1CT}$ ) [48]. The equivalent circuit for these Nyquist plots is also shown in Fig. 7. Impedance parameters  $R_{1CT}$  and  $R_{2CT}$  along with series resistance  $R_s$  of the two DSSCs can be extracted from these equivalent circuits.

The Bode phase plots of EIS spectra are shown in Fig. 8. In a Bode

phase plot complex impedance data are plotted as phase angle vs. frequency [48]. A Bode phase plot shows frequency peaks of the charge transfer process at the TiO<sub>2</sub>/electrolyte interface. The characteristic frequency peak for the reference DSSC with pristine photoanode, (a) (P25NP/P25NP/P25NP) and the DSSC with (d) (P25NP/(P25 + TiO<sub>2</sub> NF + Ag NWs)/P25NP) composite photoanode are 8.69 Hz and 12.65 Hz respectively. It is clear that the characteristic frequency peak ( $f_{max}$ ) has been shifted to a lower frequency when Ag NWs and TiO<sub>2</sub> NFs are incorporated into the middle layer of the photoanode. From  $f_{max}$  value the electron lifetimes ( $\tau_e$ ) can be obtained using the following equation [48],

The impedance parameters  $R_{1CT}$ ,  $R_{2CT}$ ,  $f_{max}$  along with the photovoltaic parameters and  $\tau_e$  extracted from EIS measurements are tabulated in Table 2.

As seen from Table 2, there is a decrease in  $R_{1CT}$  and  $R_{2CT}$  values for the DSSC with composite photoanode (d) P25NP/(P25NP + TiO<sub>2</sub> NF + Ag NW)/P25NP compared to the DSSC with reference photoanode (a) P25NP/P25NP/P25NP. The decrease in  $R_{1CT}$  implies that the increase in the oxidation rate and the redox mediator favours the electron collection at the Pt counter electrode [48–50]. The decrease in the resistance value of  $R_{2CT}$  with respect to the reference cell suggests that the incorporation of Ag NWs has improved the charge transfer process across the composite photoanode (d) and the electrolyte. This is very likely due to the better Ag NWs mediated conductivity. The improvement in electron transfer process at TiO<sub>2</sub>/electrolyte interface contributes to the overall improvement in the electron transfer process in the photoanode. The decrease in  $R_{2CT}$  also implies that the electrons released by the redox couple reach the oxidized dye molecule easily.

From Table 2, it is evident that the electron lifetime is highest for the DSSC with composite photoanode (d) P25NP/(P25NP + TiO<sub>2</sub> NF + Ag NWs)/P25NP. This means that in this photoanode, electrons diffuse and transfer more easily. Higher electron lifetime also implies reduced recombination of photoelectrons between TiO<sub>2</sub> photoanode and the electrolyte, which contributes to the enhancement in  $J_{sc}$  leading to overall efficiency enhancement.

#### 4. Conclusion

In this work, the effect of incorporating Ag NWs and TiO<sub>2</sub> NFs into a tri-layered photoanode of the DSSC has been investigated. By incorporating Ag NWs and TiO<sub>2</sub> NFs with optimized concentration only to the middle layer of the tri-layer photoanode, a remarkable efficiency enhancement of 45.6% has been obtained with respect to reference tri-layered DSSC with pristine, tri-layer P25NP/P25NP/P25NP photoanode with the same total thickness (~28  $\mu$ m). The observed efficiency enhancement as shown by  $J$ - $V$  characteristics, IPCE measurements and EIS measurements, is evidently due to the increased short circuit photocurrent density which can be attributed to the increase in light harvesting due to (a) improved light absorption by multiple scattering events by TiO<sub>2</sub> nanofibres (NF) within the composite multi-layer structure and (b) enhanced light absorption due to the local surface plasmon resonance (LSPR) effect by Ag nanofibres (AgNF) in the composite tri-layer photoanode.

**Table 2**

Charge-transfer resistance of the Pt/electrolyte interface ( $R_{1CT}$ ), charge-transfer resistance of the TiO<sub>2</sub>/electrolyte ( $R_{2CT}$ ) interface, characteristic frequency peak ( $f_{max}$ ) and electron recombination life times ( $\tau_e$ ), along with photovoltaic parameters of DSSCs with tri-layer photoanodes (a) (P25NP/P25NP/P25NP) and (d) (P25NP/(P25NP + TiO<sub>2</sub> NF + Ag NWs)/P25NP) configured on FTO/TiO<sub>2</sub> CL.

DSSC TiO <sub>2</sub> Photoanode Configuration	PCE (%)	$J_{sc}$ (mAcm <sup>-2</sup> )	$R_{1CT}$ ( $\Omega$ )	$R_{2CT}$ ( $\Omega$ )	$f_{max}$ (Hz)	$\tau_e$ (ms)
(a) P25NP/P25NP/P25NP (reference)	6.69	14.3	15.3	7.89	8.6851	18.3
(d) P25NP/(P25NP + TiO <sub>2</sub> NF + AgNW)/P25NP	9.74	19.8	7.56	4.32	12.649	12.6

## Acknowledgement

The authors gratefully acknowledge the financial support provided by the NSF under the Grant No NSF/RG/2018/BS/01.

## References

- [1] B. O'Regan, M. Grätzel, A low-cost, high-efficiency solar cell based on dye-sensitized colloidal TiO<sub>2</sub> films, *Nature* 353 (1991) 737–740.
- [2] K. Hara, H. Arakawa, Dye-sensitized solar cells, in: Y. Tachibana, K. Hara, K. Sayama, H. Arakawa (Eds.), *Handbook of Photovoltaic Science and Engineering*, John Wiley & Sons Ltd, Chichester, 2010, pp. 664–670.
- [3] G.K. R. Senadeera, S. Kobayashi, T. Kitamura, Y. Wada, S. Yanagida, Versatile preparation method for mesoporous TiO<sub>2</sub> electrodes suitable for solid-state dye sensitized photocells, *Bull. Mater. Sci.* 28 (6) (2005) 635–641.
- [4] M. Grätzel, Solar energy conversion by Dye-sensitized photovoltaic cells, *Inorg. Chem.* 44 (2005) 6841–6851.
- [5] R. Amadelli, R. Argazzi, C.A. Bignozzi, F. Scandola, Design of antenna-sensitizer polynuclear complexes. Sensitization of titanium dioxide with [Ru(bpy)<sub>3</sub>](CN)<sub>2</sub>]2RU(bPY(COO)<sub>2</sub>)<sub>2</sub><sup>-</sup>, *J. Am. Chem. Soc.* 1 (12) (1990) 7099–7103.
- [6] S. Mathew, A. Yella, P. Gao, R. Humphry-Baker, B.F.E. Curchod, N. Ashari-Astani, I. Tavernelli, U. Rothlisberger, Md. K. Nazeeruddin, M. Grätzel, Dye-sensitized solar cells with 13% efficiency achieved through the molecular engineering of porphyrin sensitizers, *Nat. Chem.* 6 (242) (2014) 242–247.
- [7] N. Koumura, Z. Wang, S. Mori, M. Miyashita, E. Suzuki, K. Hara, Alkyl-functionalized organic dyes for efficient molecular photovoltaics, *J. Am. Chem. Soc.* 1 (28) (2006), 14256–6851.
- [8] M. Nazeeruddin, A. Kay, I. Rodicic, R. Humphry-Baker, E. Müller, P. Liska, Conversion of light to electricity by cis-XzBis(2,20-bipyridyl)-4,40-dicarboxylate)ruthenium(II) charge transfer sensitizers (X = Cl-, Br-, I-, CN-, and SCN-) on nanocrystalline TiO<sub>2</sub> electrodes, *J. Am. Chem. Soc.* 115 (1993) 6382–6390.
- [9] M.A.K.L. Dissanayake, C.A. Thotawatthage, G.K.R. Senadeera, T.M.W.J. Bandara, W.J.M.J.S.R. Jayasundera, B.E. Mellander, Efficiency enhancement by mixed cation effect in dye-sensitized solar cells with PAN based gel polymer electrolyte, *J. Photochem. Photobiol., A* 246 (2012) 29–35.
- [10] H. Wang, X. Zhang, F. Gong, G. Zhou, Z. Wang, Novel ester functionalized solid-state electrolyte for highly efficient all-solid state dye-sensitized solar cells, *Adv. Mater.* 24 (2012) 121–124.
- [11] M.A.K.L. Dissanayake, W.N.S. Rupasinghe, V. A. Seneviratne, C.A. Thotawatthage, G.K.R. Senadeera, Optimization of iodide ion conductivity and nano filler effect for efficiency enhancement in polyethylene oxide (PEO) based dye sensitized solar cells, *Electrochim. Acta* 145 (2014) 319–326.
- [12] M.A.K.L. Dissanayake, H.K.D.M.N.R. Divarathne, C.A. Thotawatthage, C.B. Dissanayake, G.K.R. Senadeera, B.M.R. Bandara, Dyesensitized solar cells based on electrospunpolyacrylonitrile (PAN) nanofibre membrane gel electrolyte, *Electrochim. Acta* 130 (2014) 76–81.
- [13] S. Chuangchote, T. Sagawa, S. Yoshikawa, Efficient dye-sensitized solar cells using electrospun TiO<sub>2</sub>nanofibers as a light harvesting layer, *App.Phys. Lett.* 93 (2008) 033310–033313.
- [14] W. HoJung, N.S. Kawak, T., S. Hwang, K.B. Yi, Preparation of highly porous TiO<sub>2</sub> nanofibers for dye-sensitized solar cells (DSSCs) by electro-spinning, *Appl. Surf. Sci.* 26 (15) (2012) 343–352.
- [15] P. Roy, S., P. Abau, P. Schmuki, TiO<sub>2</sub> nanotubes in dye-sensitized solar cells: higher efficiencies by well-defined tube tops, *Electrochem. Commun.* 12 (7) (2010) 949–951.
- [16] D.J. Yang, H. Park, S.J. Chao, H.G. Kim, W.Y. Choul, TiO<sub>2</sub>-nanotube-based dye-sensitized solar cells fabricated by an efficient anodic oxidation for high surface area, *J. Phys. Chem. Solid.* 69 (5–6) (2008) 1272–1275.
- [17] D. Maheswari, D. Sreenivasan, Review of TiO<sub>2</sub> nanowires in dye sensitized solar cell, *Appl. Sol. Energy* 51 (2) (2015) 112–116.
- [18] L. Xiao, J. Xu, X. Liu, Y. Zhang, B. Zhang, J. Yao, S. Dai, Z. Tan, X. Pan, Mesoporous TiO<sub>2</sub> nanowire film for dye-sensitized solar cell, *J. Nanosci. Nanotechnol.* 16 (6) (2016) 5605–5610.
- [19] Y.Y. Lee, H. E. Shall, Ultra-high aspect ratio titania nanoflakes for dye-sensitized solar cells, *Appl. Surf. Sci.* 426 (31) (2017) 1263–1270.
- [20] How light trapping surfaces will boost solar cell efficiency [online]. Available from: <https://www.technologyreview.com/s/510016/how-light-trapping-surfaces-will-boost-solar-cell-efficiency/>[Accessed 22nd October, 2017].
- [21] K.S. Swathy, P.A. Abraham, N.R. Panicker, N.C. Pramanik, S.K. Jacob, Nanostructured anatasetitania spheres as light scattering layer in Dye-sensitized solar cells, *Proc. Technol.* 24 (2016) 767–773.
- [22] S. Ito, Md. K. Nazeeruddin, P. Liska, P. Comte, R. Charvet, P. Péchy, M. Jirousek, A. Kay, S.M. Zakeeruddin, M. Grätzel, Photovoltaic characterization of dye-sensitized solar cells: effect of device masking on conversion efficiency, *Prog. Photovoltaics Res. Appl.* 14 (2006) p589–601.
- [23] Hua Xu, Xiaoqing Chen, Shuxin Ouyang, Tetsuya Kako, Jinhua Ye, Size-dependent mie's scattering effect on TiO<sub>2</sub> spheres for the superior photoactivity of H<sub>2</sub> evolution, *J. Phys. Chem. C* 116 (5) (2012) 3833.
- [24] P. Zhu, A. Sreekumaran Nair, Shengyuan Yang, Shengjie Peng, Seeram Ramakrishna, Which is a superior material for scattering layer in dye-sensitized solar cells— electrospun rice grain- or nanofiber-shaped TiO<sub>2</sub>, *J. Mater. Chem.* 21 (2011) 12210–12212.
- [25] P. Joshi, L. Zhang, D. Davoux, Z. Zhu, D. Galipeau, H. Fong, Q. Qiao, Composite of TiO<sub>2</sub> nanofibers and nanoparticles for dye-sensitized solar cells with significantly improved efficiency, *Energy Environ. Sci.* 3 (2010) 1507.
- [26] M.A.K.L. Dissanayake, H.K.D.W.M.N. Divarathnaa, C.B. Dissanayake, G.K.R. Senadeera, P.M.P.C. Ekanayake, C.A. Thotawatthage, An innovative TiO<sub>2</sub> nanoparticle/nanofibre/nanoparticle, three layer composite photoanode for efficiency enhancement in dye-sensitized solar cells, *J. Photochem. Photobiol. Chem.* 322 (2016) 110–118.
- [27] M.A.K.L. Dissanayake, H.N.M. Sarangika, G.K.R. Senadeera, K.D.W.M.N.R. Divarathna, M.P.C. Ekanayake, Application of a nanostructured, tri-layer TiO<sub>2</sub>photoanode for efficiency enhancement in quasi-solid electrolyte-based dye-sensitized solar cells, *J. Appl. Electrochem.* 47 (2017) 1239–1249.
- [28] M.A.K.L. Dissanayake, T. Jaseetharan, G.K.R. Senadeera, C.A. Thotawatthage, A novel, PbS:Hg quantum dot-sensitized, highly efficient solar cell structure with triple layered TiO<sub>2</sub> photoanode, *Electrochim. Acta* 269 (2018) 172.
- [29] H.J. Koo, J. Park, B. Yoo, K. Kim, N.G. Park, Size-dependent scattering efficiency in dye-sensitized solar cell, *Inorg. Chim. Acta.* 361 (2008) 677–683.
- [30] G.K. Mor, K. Shankar, M. Paulose, O.K. Varghese, C.A. Grimes, Use of highly-ordered TiO<sub>2</sub> nanotube Arrays in dye-sensitized solar cells, *Nano Lett.* 6 (2006) 215–218.
- [31] V. Tan, Y.Y. J. Wu, Dye-sensitized solar cells based on anatase TiO<sub>2</sub> nanoparticle/nanowire composites, *Phys. Chem. B* 110 (2006) 15932–15938.
- [32] Y. Ohsaki, N. Masaki, T. Kitamura, Y. Wada, T. Okamoto, T. Sekino, K. Niihara, S. Yanagida, Phys. Chem. Dye-sensitized TiO<sub>2</sub> nanotube solar cells: fabrication and electronic characterization, *Chem. Phys.* 7 (2005) 4157–4163.
- [33] M. Law, L.E. Greene, J.C. Johnson, R. Saykally, P.D. Yang, Nanowire dye-sensitized solar cells, *Nat. Mater.* 4 (2005) 455–459.
- [34] H. Kokubo, B. Ding, T. Naka, H. Tsuchihira, S. Shiratori, Multi-core cable-like TiO<sub>2</sub> nanofibrous membranes for dye-sensitized solar cells, *Nanotechnology* 18 (2007), 165604.
- [35] M.Y. Song, Y.R. Ahn, S.M. Jo, D.Y. Kim, J.P. Ahn, Effects of down conversion luminescent film in dye-sensitized solar cells, *Appl. Phys. Lett.* 87 (2005), 113113.
- [36] M.A.M. Ziyen, M.A.K.L. Dissanayake, U.L. Zainudeen, G.K.R. Senadeera, C.A. Thotawatthage, Study of dye-sensitized solar cells with TiO<sub>2</sub> nanoparticles/nanofibers composite electrode using photovoltaic and EIS measurements, in: *Proc.Solar Asia 2018 International Conference*, Kandy, Sri Lanka, 4-6 January, 2018, pp. 163–168. <http://nifs.ac.lk>
- [37] J.M.K.W. Kumari, N. Sanjeevadarshini, M.A.K.L. Dissanayake, G.K.R. Senadeera, C.A. Thotawatthage, The effect of TiO<sub>2</sub> photoanode film thickness on photovoltaic properties of dye-sensitized solar cells, *Ceylon J. Sci.* 45 (1) (2016) 33–41.
- [38] K. Marchuk, K.A. Willets, Localized surface plasmons and hot electrons, *Chem. Phys. Invit. Perspect.* 445 (2014) 95–104.
- [39] D.M. Schaadt, B. Feng, E.T. Yu, Enhanced semiconductor optical absorption via surface plasmon excitation in metal nanoparticles, *Appl. Phys. Lett.* 86 (2005), 063106.
- [40] M. Ihara, K. Tanaka, K. Sakaki, I. Honma, K. Yamada, Enhancement of the absorption coefficient of cis-(NCS)<sub>2</sub> bis(2,2'-bipyridyl)-4,4'-dicarboxylate) ruthenium(II) dye in dye-sensitized solar cells by a silver island film, *J. Phys. Chem. B* 101 (1997) 5153–5157.
- [41] M.K. Gangishetty, K.E. Lee, R.W. Scott, T.L. Kelly, Plasmonic enhancement of dye sensitized solar cells in the red-to-near-infrared region using triangular core-shell Ag@SiO<sub>2</sub> nanoparticles, *ACS Appl. Mater. Interfaces* 5 (2013) 11044–11051.
- [42] S.K. Cushing, J. Li, F. Meng, T.R. Senty, S. Suri, M. Zhi, M. Li, A.D. Bristow, N. Wu, Photocatalytic activity enhanced by plasmonic resonant energy transfer from metal to semiconductor, *J. Am. Chem. Soc.* 134 (2012) 15033–15041.
- [43] P.J. Schuck, Nanoimaging: hot electrons go through the barrier, *Nat. Nanotechnol.* 8 (2013) 799–800.
- [44] C. Yang, Y. Tang, Z. Su, Z. Zhang, C. Fang, Preparation of silver nanowires via a rapid, scalable and green pathway, *J. Mater. Sci. Technol.* 31 (2015) 16–22.
- [45] E.V. Ferry, J.N. Munday, H.A. Atwater, Design considerations for plasmonic photovoltaics, *Adv. Mater.* 22 (2010) 4794–4808.
- [46] M.A.K.L. Dissanayake, J.M.K.W. Kumari, G.K.R. Senadeera, C.A. Thotawatthage, Efficiency enhancement in plasmonic dye-sensitized solar cells with TiO<sub>2</sub> photoanodes incorporating gold and silver nanoparticles, *J. Appl. Electrochem.* 46 (2016) 47–58.
- [47] M.G.C.M. Kumari, C.S. Perera, B.S. Dassanayake, M.A.K.L. Dissanayake, G.K.R. Senadeera, Plasmon enhanced dye sensitized solar cell performance using TiO<sub>2</sub>/Ag NW nanocomposite photoanode, in: *Proc. Solar Asia 2018 International Conference*, Kandy, Sri Lanka, 4-6 January, 2018, pp. 179–184. <http://nifs.ac.lk>
- [48] Q. Wang, J. Moser, M. Graetzel, Electrochemical impedance spectroscopic analysis of dye-sensitized solar cells, *J. Phys. Chem. B* 109 (2005) 14945–14953.
- [49] H. Hoppe, N.S. Saricicfci, Organic solar cells: an overview, *J. Mater. Res.* 19 (2004) 1924–1945.
- [50] M.A.K.L. Diasanayakea, G.K.R. Senadeera, H.N.M. Sarangikaa, P.M.P.C. Ekanayake, C.A. Thotawatthage, H.K.D.W.M.N.R. Divarathna, J.M.K.W. Kumari, TiO<sub>2</sub> as a low cost, multi functional material, *Mater. Today: Proceedings* 3S (2016) S40–S47.
- [51] A.E. Shalan, M.M. Rashad, Youhai Yu, Mónica Lira-Cantú, M.S.A. Abdel-Mottaleb, A facile low temperature synthesis of TiO<sub>2</sub> nanorods for high efficiency

- dye sensitized solar cells, *Appl. Phys. A* 110 (2013) 111–122 (*Material Science and Processing* ).
- [52] Nak Cheon Jeong, Chaiya Prasittichai, Joseph T. Hupp, Photocurrent enhancement by surface plasmon resonance of silver nanoparticles in highly porous dye-sensitized solar cells, *Langmuir* 27 (2011) 14609–14614.
- [53] P.S. Chandrasekhar, Hytham Elbohy, Bjorn Vaggensmith, Ashish Dubey, Khan Mamun Reza, Vamsi K. Komarala, Qiquan Qiao, Plasmonic silver nano-wires for higher efficiency dye-sensitized solar cells, *Mater. Today Energy* 5 (2017) 237–242.
- [54] William R. Erwin, Holly F. Zarick, Eric M. Talbert, Rizia Bardhan, Light trapping in mesoporous solar cells with plasmonic nanostructures, *Energy Environ. Sci.* 9 (2016) 1577–1602.